PUBLICATION III

Influence of Cr alloying on the microstructure of thermally sprayed quasicrystalline Al-Cu-Fe coatings

In: Intermetallics 2003. Vol. 11, pp. 879–891.

Available online at www.sciencedirect.com
SCIENCE DIRECT®
ELSEVIER
Intermetallics 11 (2003) 879–891
Intermetallics
www.elsevier.com/locate/intermet

Influence of Cr alloying on the microstructure of thermally sprayed quasicrystalline Al–Cu–Fe coatings

Elina Huttunen-Saarivirta[a,*], Erja Turunen[b], Marke Kallio[c]

[a]Tampere University of Technology, Institute of Materials Science, PO Box 589, Fin-33101 Tampere, Finland
[b]VTT Technical Research Centre of Finland, Surface Engineering and Laser Processing, PO Box 1703, Fin-02044 VTT, Finland
[c]VTT Technical Research Centre of Finland, Materials and Chemicals, Hermiankatu 8 G, PO Box 16071, Fin-33101 Tampere, Finland

Received 7 April 2003; accepted 8 May 2003

Abstract

The present work reports the structural development of Al–Cu–Fe and Al–Cu–Fe–Cr coatings deposited by the high velocity oxy-fuel thermal spraying process and the influence of Cr alloying on the phase selection of Al–Cu–Fe coatings at various deposition temperatures. The porosity levels of the Al–Cu–Fe and Al–Cu–Fe–Cr coatings of the study are demonstrated to be lower than those reported for corresponding plasma-sprayed coatings. The results show that high velocity oxy-fuel spraying technique produces Al–Cu–Fe coatings that are phase structurally similar to plasma-sprayed Al–Cu–Fe coatings reported in literature. Al–Cu–Fe coatings are composed of a crystalline β-AlFe phase and a quasicrystalline i-$Al_{65}Cu_{20}Fe_{15}$ phase as well as an oxidised form of either or both of these phases. Addition of Cr to Al–Cu–Fe alloys introduces coatings that are made up of the crystalline θ-Al_2Cu phase and two quasicrystalline phases, the i_1-$Al_{80}Cr_{13.5}Fe_{6.5}$ and i_2-$Al_{13}Cr_3Cu_4$ phases. The formation of these icosahedral phases in Al–Cu–Fe–Cr alloys has not been reported before, although the occurrence of quasicrystal approximants with compositions close to those of the i_1-$Al_{80}Cr_{13.5}Fe_{6.5}$ and i_2-$Al_{13}Cr_3Cu_4$ phases has been demonstrated. On the basis of our results we propose that the icosahedral phase structure is greatly stabilised by the Cr addition to Al–Cu–Fe alloys.

Keywords: A. Multiphase intermetallics; B. Phase identification; C. Coatings; D. Microstructure

1. Introduction

During the early 1980s, a new material group with a long-range orientational but no translational order emerged [1]. Until then, a dichotomy between amorphous and crystalline materials had prevailed in the realm encompassing the structure of materials. The discovery of these quasicrystalline materials exhibiting an atomic structure somewhere between that of amorphous and crystalline materials, thus, significantly widened the scope of the structural foundation of materials.

Up to now, quasicrystalline phases with fivefold, eightfold, tenfold or even twelvefold rotational symmetries have been observed in over a hundred different metal alloy systems. Besides being theoretically interesting due to their complicated atomic structure, the unique properties of quasicrystalline materials—high hardness [2,3], a low surface energy [4–6] accompanied by a low coefficient of friction [5,7], good corrosion [4] and wear [8] resistance, low electrical and thermal conductivity [9–13] and unusual optical properties [14], to name a few—make them tempting to many practical purposes, too. However, the utilisation of quasicrystalline materials in bulk form is often compromised by their brittleness [2,15,16]. Therefore, quasicrystalline materials with these extreme surface properties are at their best in coating applications, when used in combination with more ductile substrate materials, which, in turn, provide the bulk properties.

In tribological applications, Al–Cu–Fe and Al–Cu–Fe–Cr are the most often utilised quasicrystalline materials. They are generally used in the form of thick coatings, produced by plasma spraying [8,17–21]. In this study, Al–Cu–Fe and Al–Cu–Fe–Cr thick coatings are deposited by a high velocity oxy-fuel (HVOF) spraying technique. Besides this thermal spraying technique not very much used to yield quasicrystalline coatings, the

* Corresponding author. Tel.: +358-3-31152912; fax: +358-3-31152330.
E-mail address: elina.huttunen-saarivirta@tut.fi (E. Huttunen-Saarivirta).

0966-9795/03/$ - see front matter © 2003 Elsevier Ltd. All rights reserved.
doi:10.1016/S0966-9795(03)00097-9

novelty of the present study lies in its comparative approach of the HVOF spraying of two different alloy coating, Al–Cu–Fe and Al–Cu–Fe–Cr. Although the structural development of both of these alloys during the thermal spraying process have been studied individually, no earlier reports compare their microstructures systematically by taking the influence of alloying elements and spraying parameters into account. The paper was, accordingly, motivated by the limited amount of experimental studies concerning the effect of Cr alloying on the microstructure of Al–Cu–Fe alloys, although the formation of new phases as a result of Cr alloying of Al–Cu–Fe is theoretically known. The present paper addresses the influence of chromium alloying on the microstructure of HVOF sprayed quasicrystalline Al–Cu–Fe coatings in different spraying temperatures.

The objective of the study is to tackle some aspects, which have not been completed in the earlier studies on thermally sprayed Al–Cu–Fe and Al–Cu–Fe–Cr coatings. In this study, Al–Cu–Fe and Al–Cu–Fe–Cr coatings are produced by HVOF spraying technique to gain new information on their structural development under different spraying conditions. The formed coating microstructures are compared to existing literature on the microstructures of coatings produced by other thermal spraying methods. In addition to the thermal spraying technique effects, the study aims at clarifying the role of Cr alloying in the phase selection of Al–Cu–Fe coatings at various temperatures. X-ray diffractometry (XRD), scanning electron microscopy (SEM) and analytical electron microscopy (ATEM) are used for the microstructural characterisation of Al–Cu–Fe and Al–Cu–Fe–Cr feed powders and HVOF sprayed coatings.

2. Experimental

2.1. Preparation of coatings

Al–Cu–Fe and Al–Cu–Fe–Cr coatings were applied on low carbon steel substrates by a high velocity oxy-fuel (HVOF) spraying technique. The HVOF spraying technique is a thermal spraying method, where a spray powder is fed to the gas flow of high pressure and which yields coatings of low porosity and, therefore, of good surface properties [22]. In the present study, the spray powders were commercial powders Christome F1 and A1/S, corresponding to Al–Cu–Fe and Al–Cu–Fe–Cr powders, respectively. These powders were manufactured by Saint-Gobain Advanced Ceramics SNMI, France. The composition of the Al–Cu–Fe powder, given by the manufacturer, was 40.8 wt.% Al, 41.2 wt.% Cu, 17.0 wt.% Fe and 0.8 wt.% B, which corresponds to the composition 59.6 at.% Al, 25.5 at.% Cu, 12.0 at.% Fe and 2.9 at.% B. The particle size of this powder ranged from 20 to 45 μm. In turn, the composition of the Al–Cu–Fe–Cr powder, given by the manufacturer, was 54.1 wt.% Al, 17.8 wt.% Cu, 13.0 wt.% Fe and 14.9 wt.% Cr, which corresponds to the composition 71.5 at.% Al, 10.0 at.% Cu, 8.3 at.% Fe and 10.2 at.% Cr. The particle size of this powder ranged from 20 to 53 μm.

The coatings were sprayed using a HV-2000 spray gun by Praxair Surface Technologies (USA). The gun was operated by a Model 3440 console utilising a model 1262 volumetric powder feeder by Plasmatron Pvt.Ltd (USA). A two-axis traverse unit with a rotating spindle of a 200 mm inner diameter was used to manipulate the gun and the substrates during the coating deposition. The spray distance was 300 mm in the spraying experiments of the study. In the HVOF process, nitrogen was used as a carrier gas, along with hydrogen as a fuel gas. The coatings were sprayed under two different operation conditions, varying the flow of hydrogen and oxygen and their ratio. The gas flow ratio generally determines the temperature of the flame [22], the higher oxygen content promoting the higher flame temperature. This also applied to the HVOF spraying process of the study. The thickness of the HVOF sprayed coatings also varied in the spraying experiments. The spraying conditions used in the study and the coating thicknesses are shown in Table 1.

Temperature of the sprayed particles was studied through the spraying diagnostics. SprayWatch 2i imaging system from Oseir Ltd. (Finland), designed for the quality control of industrial thermal spray processes, was used for the on-line measurements of in-flight particles' temperature in the spray. It has to be noticed that these temperature measurements conducted during the spraying experiments only recorded the surface temperature of powder particles. Due to the low thermal conductivity of the powder particles, however, the true

Table 1
HVOF spraying conditions and the resulting coating thicknesses

Spray powder alloy	Coating	O_2 (l/min)	H_2 (l/min)	H_2/O_2 (ratio)	Surface temperature of powder particles (°C)	Thickness (μm)
Al–Cu–Fe	A	235	665	2.83	1983	310
Al–Cu–Fe	B	280	620	2.21	2015	280
Al–Cu–Fe–Cr	C	235	665	2.83	2003	289
Al–Cu–Fe–Cr	D	280	620	2.21	2011	284

temperature of the inner part of particles cannot be evaluated. For the same reason, the temperature difference measured between the surfaces of particles does not correspond to the true temperature difference between the inner parts of the particles. The surface temperature of powder particles, therefore, only gives a rough approximation about the scale of temperature the powder particles reach during the spraying process.

2.2. Microstructural characterisation of coatings

The microstructural characterisation of Al–Cu–Fe and Al–Cu–Fe–Cr coatings was performed by X-ray diffraction (XRD) measurements, scanning electron microscopy (SEM) and analytical transmission electron microscopy (ATEM). The XRD measurements were carried out using a model Diffrac 500 diffractometer by Siemens (Germany) and copper K_α radiation with the wavelength of 0.1540501 nm. The XRD analyses were performed with powder samples. Thus, the studied coatings were stripped off their substrates and crushed into powder form in a mortar. In addition to the powder coating samples, the feed powder was characterised by XRD in order to reveal the possible phase transitions introduced by the coating process. The microstructure of the feed powder and the sprayed coatings was also studied with a scanning electron microscope model XL30 by Philips (The Netherlands), equipped with an energy dispersive spectrometer (EDS) model DX-4 by EDAX International (USA). SEM examination was used for the coating thickness determination as well, the given coating thicknesses being average values from ten individual measurements. Cross-sectional samples were used in the SEM studies. The feed powder and the sprayed coatings were further examined by an analytical transmission electron microscope JEM 2010 by Jeol (Japan) equipped with a Noran Vantage energy dispersive spectrometer by ThermoNoran (The Netherlands). The ATEM was operated at an accelerating voltage of 200 kV. ATEM examination was conducted for powdery samples; the coating samples were prepared similarly as for the XRD analyses.

3. Results

3.1. Microstructural characterisation of Al–Cu–Fe coatings

Fig. 1 shows the XRD patterns for the Al–Cu–Fe feed powder and the HVOF sprayed coatings A and B. The Al–Cu–Fe spray powder (Fig. 1a) was detected to represent a two-phase structure, consisting of the

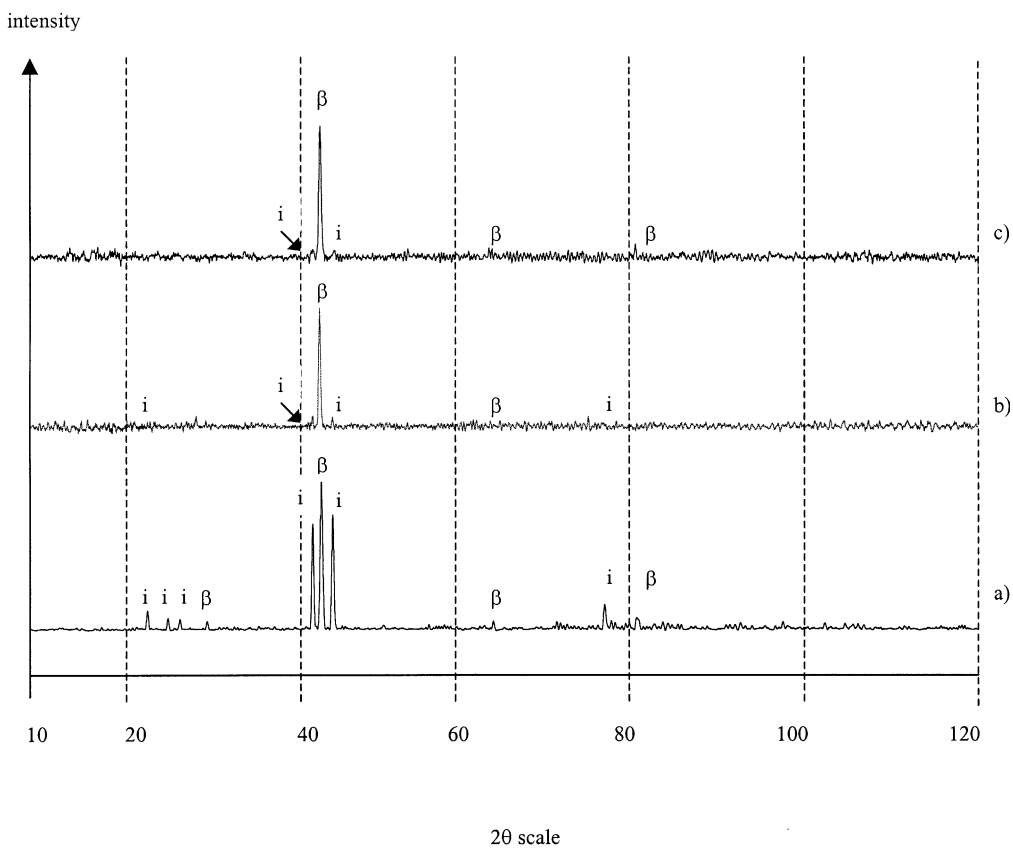

Fig. 1. XRD patterns for the (a) Al–Cu–Fe spray powder, (b) Al–Cu–Fe coating A sprayed with the lower spraying temperature, (c) Al–Cu–Fe coating B sprayed with the higher spraying temperature. i denotes the icosahedral $Al_{65}Cu_{20}Fe_{15}$ phase, β stands for the cubic AlFe phase.

quasicrystalline icosahedral i-$Al_{65}Cu_{20}Fe_{15}$ phase and the crystalline cubic β-AlFe phase. According to the manufacturer, the feed powder is almost completely quasicrystalline. However, the quantitative analysis of the amount of i-$Al_{65}Cu_{20}Fe_{15}$ and β-AlFe phases in the feed powder by comparing their peak heights in the XRD spectrum is very suspect due to the complex atomic structure and scattering phenomena associated with the quasicrystalline i-$Al_{65}Cu_{20}Fe_{15}$ phase. Due to this, the relative amount of these phases could not be evaluated on the basis of the XRD data.

The HVOF sprayed Al–Cu–Fe coatings A (Fig. 1b) and B (Fig. 1c) were composed of the same two phases as the feed powder, i-$Al_{65}Cu_{20}Fe_{15}$ and β-AlFe. Comparison of the XRD spectrum of Al–Cu–Fe coating A to that of Al-Cu-Fe coating B revealed them to be almost identical. The only registered differences were a somewhat higher intensity of peaks and their greater amount in the XRD trace of coating A, deposited with lower spraying temperature. As for the divergences between the XRD spectra of HVOF sprayed Al–Cu–Fe coatings A and B and that of the feed powder, in turn, more significant dissimilarities could be discovered. The relative intensity of i-$Al_{65}Cu_{20}Fe_{15}$ peaks was dramatically decreased during the spraying process, while that of β-AlFe peaks was not altered remarkably. Besides the lowered intensity of i-$Al_{65}Cu_{20}Fe_{15}$ peaks, their number was also reduced due to the spraying process, the lowest-intensity peaks being erased from the XRD spectra. These findings strongly suggest the formation of the β-AlFe phase to be promoted by the spraying process at the expense of the i-$Al_{65}Cu_{20}Fe_{15}$ phase.

The Al–Cu–Fe feed powder consisted of spherical particles, as shown in Fig. 2a. The overall composition of the feed powder was determined to be 56.3 at.% Al, 29.3 at.% Cu and 14.5 at.% Fe. Thus, the composition of the feed powder was slightly shifted towards lower aluminium contents from the composition given by the manufacturer. No boron was observed at all; this is clearly explained, however, by the thick beryllium window of the EDS detector. SEM studies indicated Al–Cu–Fe powder particles to be composed of two phases. The lighter phase accounted for the phase with lower aluminium content, which is the β-AlFe phase. Its composition was determined to be 58.8 at.% Al, 29.6 at.% Cu and 11.5 at.% Fe. The darker phase, in contrast, corresponded to the i-$Al_{65}Cu_{20}Fe_{15}$ phase, the composition of which was 63.9 at.% Al, 22.3 at.% Cu and 13.8 at.% Fe. According to the SEM studies, neither of the phases showed an overwhelming majority in the powder microstructure, but the phases were evaluated to be present in almost equal amounts.

Fig. 2b and c shows the microstructures of Al–Cu–Fe coatings A and B, respectively. Like the feed powder, the coatings were composed of two phases, i-$Al_{65}Cu_{20}Fe_{15}$ and β-AlFe. In both coatings A and B, the β-AlFe phase was the major phase. It was observed to construct the basic coating structure, since the coating lamellas were mainly composed of the β-AlFe phase. The composition of the β-AlFe phase somewhat deviated in the studied two coating structures. In the coating A, the composition of the β-AlFe phase was 51.0 at.%

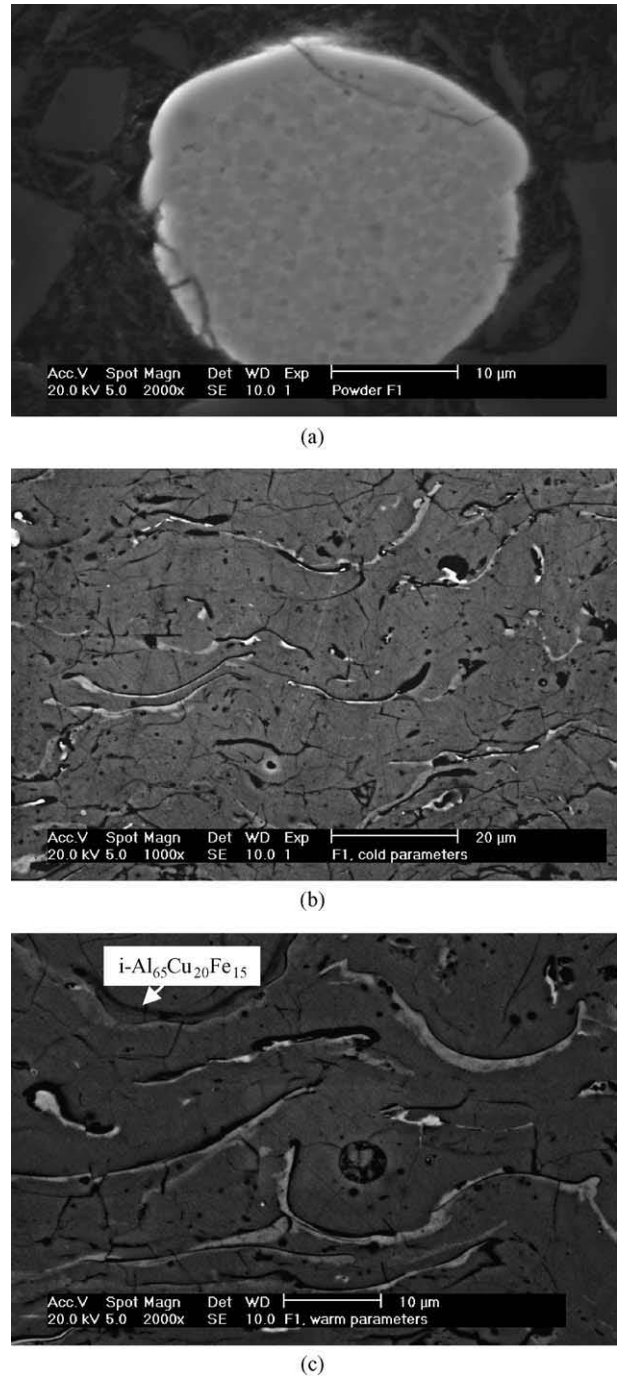

Fig. 2. SEM photographs showing the microstructural details of Al–Cu–Fe feed powder and HVOF sprayed coatings. (a) The morphology and microstructure of the Al–Cu–Fe feed powder F1. (b) The microstructure of the Al–Cu–Fe coating A deposited with the lower spraying temperature. (c) The microstructure of the Al–Cu–Fe coating B deposited with the higher spraying temperature.

Al, 32.1 at.% Cu and 16.9 at.% Fe, while in the coating B it was 43.6 at.% Al, 45.1 at.% Cu and 11.3 at.% Fe. In contrast, the composition of the minor quasicrystalline i-$Al_{65}Cu_{20}Fe_{15}$ phase was almost identical in the studied coatings; in the coating A it was 61.8 at.% Al, 26.0 at.% Cu and 12.2 at.% Fe, and in the coating B it was 61.5 at.% Al, 25.9 at.% Cu and 12.5 at.% Fe. The quasicrystalline i-$Al_{65}Cu_{20}Fe_{15}$ was often located near the coating lamella surfaces, as there the cooling rate is the highest. In addition to these two phases, i-$Al_{65}Cu_{20}Fe_{15}$ and β-AlFe, an oxygen-containing phase could be resolved between the coating lamellas. The phase was not pure aluminium oxide, but contained all the alloy elements. The oxygen-containing phase did not cause peaks in the XRD data, further confirming the absence of pure aluminium oxide. The composition of the oxygen-containing phase varied widely, from approximately 27 at.% O to 53 at.% O, with also varying amounts of other elements. Thus, based on the SEM studies, it cannot be said whether the oxidised phase forms from the β-AlFe phase or from the i-$Al_{65}Cu_{20}Fe_{15}$ phase or even from both of them.

Besides the phase structure, the influence of spraying temperature on the microstructure of Al–Cu–Fe coatings can be evaluated from Fig. 2b and c. The microstructure of Al–Cu–Fe coating A sprayed with lower spraying temperature is shown in Fig. 2b. All the powder particles were not completely melted during the spraying process. Accordingly, a perfectly lamellar and dense coating structure was not formed. Instead, porosity was incorporated in the coating. When the higher spraying temperature was utilised, the feed powder particles were more efficiently melted, leading to a reduced level of porosity in coating B. Higher spraying temperature was therefore noticed to promote the formation of somewhat denser coating structure as the lower spraying temperature. Similarly, higher spraying temperature was observed to favour the oxide layer build-up on lamella boundaries. It is worth noting that although oxidation generally occurs due to increased spraying temperature, quite a heavy oxidation of Al–Cu–Fe spray powder took place during the deposition process independently of which spraying temperature was used. However, the oxide layers were thicker, when higher deposition temperature was employed.

In the ATEM characterisation, the results of XRD and SEM examinations concerning the structure of Al–Cu–Fe coatings A and B were confirmed. The powder particles, in turn, could not be properly studied by ATEM due to their relatively large size and, accordingly, great thickness. Fig. 3 shows the microstructure of the Al–Cu–Fe coating A studied by ATEM. The coating lamellas are clearly distinguished in Fig. 3a and b, as the light areas of oxygen-containing phase separate individual lamellas. The lamellas were mainly composed of the β-AlFe phase grains, the diameter of which generally varied in the range from 30 to 140 nm (Fig. 3c). This rather small grain size was reflected in the occurrence of rings in the electron diffraction pattern (Fig. 3d). Still, greater grains of the β-AlFe phase also existed in the coating structure (with their electron diffraction patters constituting of spots, as demonstrated in Fig. 3e). Besides the presence of the crystalline β-AlFe phase, the quasicrystalline i-$Al_{65}Cu_{20}Fe_{15}$ phase was identified in the structure of coating A. The grains of the icosahedral i-$Al_{65}Cu_{20}Fe_{15}$ phase were revealed by TEM studies to be mainly located near the lamella boundaries (Fig. 3a, b and f). These observations also hold for the Al–Cu–Fe coating B.

In addition to the microstructural features of the studied coatings, ATEM exploration also provided information on their phase compositions. In the Al–Cu–Fe coating A, the composition of the major β-AlFe phase was found to be 55.5 at.% Al, 35.1 at.% Cu and 9.4 at.% Fe. In the coating B, in contrast, the β-AlFe phase contained 57.4 at.% Al, 29.6 at.% Cu and 13.0 at.% Fe. As for the quasicrystalline i-$Al_{65}Cu_{20}Fe_{15}$ phase, in the coating A it was made up of 62.7 at.% Al, 26.3 at.% Cu and 11.0 at.% Fe. In the coating B, the corresponding composition was 64.7 at.% Al, 24.0 at.% Cu and 11.3 at.% Fe. Besides the composition of these main phases of the coatings, that of the oxygen-containing lamella-boundary phase could be determined. On average, it contained 53.0 at.% Al, 13.7 at.% Cu, 6.4 at.% Fe and 27.0 at.% O.

3.2. Microstructural characterisation of Al–Cu–Fe–Cr coatings

Fig. 4a shows the XRD results of the Al–Cu–Fe–Cr initial powder, where two different icosahedral phases, $Al_{80}Cr_{13.5}Fe_{6.5}$ and $Al_{13}Cr_3Cu_4$ (denoted by i_1 and i_2, respectively), were found to coexist together with a minor tetragonal θ-Al_2Cu phase. Marks of a decagonal quaternary phase could also be identified. These phases observed in the XRD curve of the feed powder perfectly match with the phase structure reported by the powder manufacturer. In the XRD spectrum, the peaks of the icosahedral phases were mostly superimposed. However, the major peak in the XRD pattern of the feed powder corresponds to the major peak of $Al_{13}Cr_3Cu_4$, suggesting it to be the major phase.

The XRD patterns of the HVOF sprayed coatings C and D (Fig. 4b and c) reveal their microstructure to be still composed of the same phases as the feed powder. However, the phase fractions were somewhat changed during the spraying process. Coating C, sprayed with lower operation temperature, showed almost equal peak heights for icosahedral phases i_1-$Al_{80}Cr_{13.5}Fe_{6.5}$ and i_2-$Al_{13}Cr_3Cu_4$ (Fig. 4b). Only the major peak of the tetragonal θ-Al_2Cu phase was visible in the XRD spectrum of the coating C, indicating its decreased quantity as

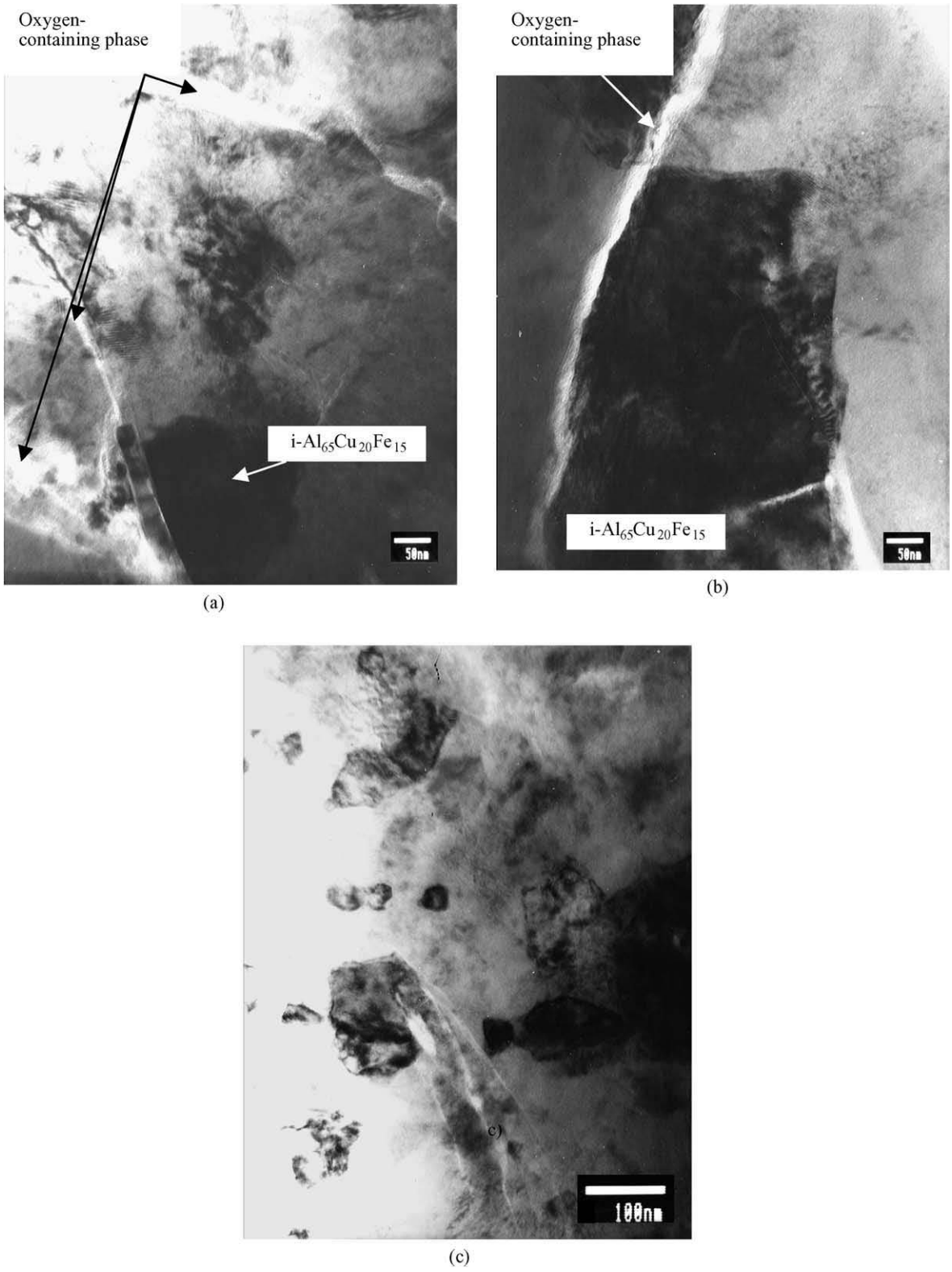

Fig. 3. Microstructure of the Al–Cu–Fe coating A sprayed with the lower spraying temperature. (a) TEM bright field (BF) image showing the coating structure from the cross-sectional perspective. Micrograph taken with the electron beam parallel to the fivefold axis of the dark grain (shown in the bottom of the figure). (b) TEM BF image showing the coating structure from the cross-sectional perspective and the icosahedral particle in the vicinity of lamella boundary. Micrograph taken with the electron beam parallel to the fivefold axis of the dark grain (shown in the bottom of the figure). (c) TEM BF image showing the grain size of the β-AlFe grains. (d) Electron diffraction pattern of the β-AlFe phase. Rings can be seen in the electron diffraction pattern, indicating a small grain size. (e) Electron diffraction pattern of the β-AlFe phase, B = [−111]. (f) Electron diffraction pattern of the icosahedral i-$Al_{65}Cu_{20}Fe_{15}$ phase, taken along the fivefold axis.

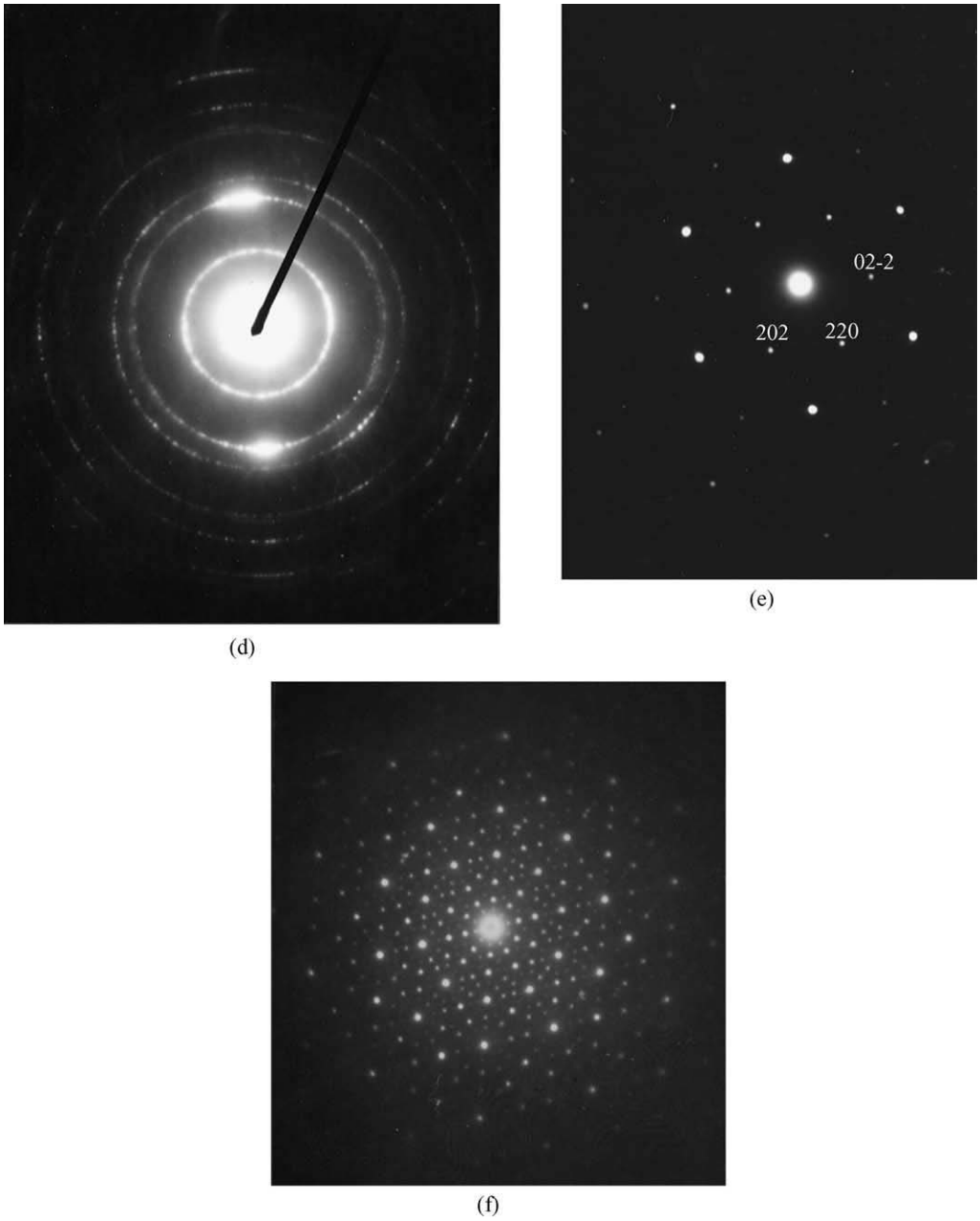

Fig. 3. (continued).

compared to the feed powder. When the spraying temperature was further increased to deposit the coating D, no marks of tetragonal θ-Al_2Cu phase could be identified in the XRD pattern (Fig. 4c), but the coating contained the icosahedral phases only. As a result of this high-temperature spraying process, the peak heights of the icosahedral phases were also changed, the major peak of the coating D corresponding to the major peak of i_1-$Al_{80}Cr_{13.5}Fe_{6.5}$.

Similarly to the Al–Cu–Fe feed powder, the Al–Cu–Fe–Cr initial powder consisted of spherical particles, as shown in Fig. 5a. The overall composition of the feed powder was determined to be 69.6 at.% Al, 10.5 at.% Cu, 9.1 at.% Fe and 10.8 at.% Cr. Thus, the composition of Al–Cu–Fe–Cr feed powder was also slightly shifted towards lower aluminium contents from the composition given by the manufacturer, like perceived for Al–Cu–Fe powder. SEM studies indicated Al–Cu–Fe–Cr powder particles to be composed of two phases: the lighter minor phase and the darker matrix. The lighter phase in the SEM photograph (Fig. 5a) corresponds to the θ-Al_2Cu phase, the composition of which was 69.7 at.% Al, 13.2 at.% Cu, 8.3 at.% Fe and 8.8 at.% Cr. The darker areas, however, were found in the elemental X-ray mapping to be made up of small copper- and iron-rich areas. Their exact boundaries could

not be determined, thus, not allowing a detailed compositional analysis. The average composition of these darker icosahedral areas, nevertheless, was 71.0 at.% Al, 6.7 at.% Cu, 10.2 at.% Fe and 12.2 at.% Cr.

A three-phase microstructure of the Al–Cu–Fe–Cr coating C can be seen in Fig. 5b, where the SEM photograph of the coating C is shown. The white areas account for the minor θ-Al_2Cu phase. The composition of this θ-Al_2Cu phase was 59.7 at.% Al, 13.3 at.% Cu, 14.1 at.% Fe and 12.9 at.% Cr. The light grey areas correspond to the copper-rich icosahedral phase i_2-$Al_{13}Cr_3Cu_4$, the composition of which was 69.0 at.% Al, 13.4 at.% Cu, 8.9 at.% Fe and 8.8 at.% Cr. The dark grey areas represent the iron-rich i_1-$Al_{80}Cr_{13.5}Fe_{6.5}$ phase. The composition of this phase was 69.2 at.% Al, 11.3 at.% Cu, 9.3 at.% Fe and 10.3 at.% Cr. In the structure of coating D, in turn, only the icosahedral phases, i_1-$Al_{80}Cr_{13.5}Fe_{6.5}$ and i_2-$Al_{13}Cr_3Cu_4$, could be well distinguished, as shown in Fig. 5c. In the coating D, these two phases were compositionally even closer to each other than in the coating C. The composition of the i_1-$Al_{80}Cr_{13.5}Fe_{6.5}$ phase, seen darker in the SEM photograph, was 68.6 at.% Al, 11.2 at.% Cu, 9.7 at.% Fe and 10.5 at.% Cr. In contrast, the composition of the lighter i_2-$Al_{13}Cr_3Cu_4$ phase was 67.9 at.% Al, 11.0 at.% Cu, 9.8 at.% Fe and 11.3 at.% Cr. The reason for the negligible compositional difference between these two phases in the coating D is suggested to be the disappearance of the θ-Al_2Cu phase at the expense of remaining icosahedral phases.

As for the influence of spraying temperature on the microstructure of Al–Cu–Fe–Cr coatings, Fig. 5b and c provides some information. As for Al–Cu–Fe coatings, higher spraying temperature tends to promote the formation of somewhat denser coatings. As compared to the Al–Cu–Fe coatings, however, the level of porosity present in coating structure seems to be somewhat greater for the Al-Cu-Fe-Cr coatings. This is explained by the greater melting point of the Al–Cu–Fe–Cr feed power compared to that of the Al–Cu–Fe feed powder.

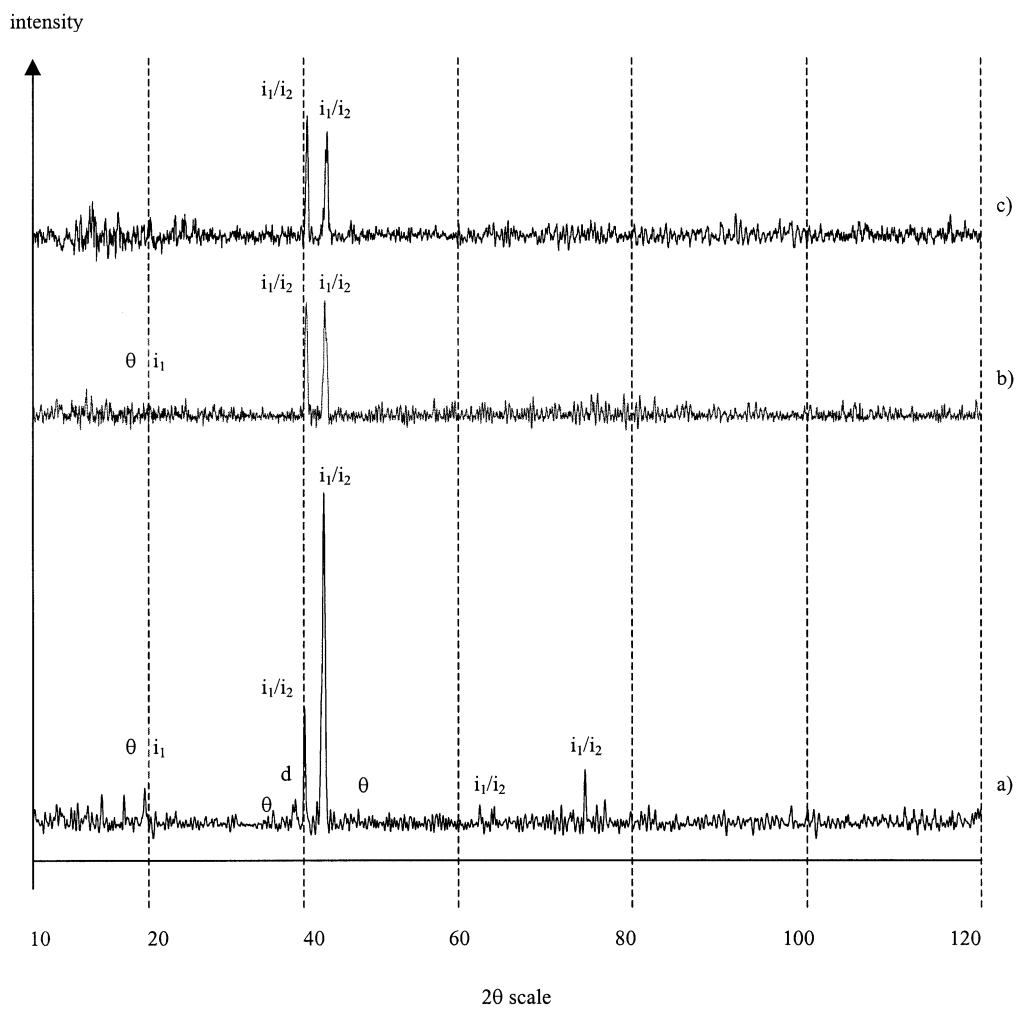

Fig. 4. XRD patterns for the (a) Al–Cu–Fe–Cr spray powder, (b) Al–Cu–Fe–Cr coating C sprayed with the lower spraying temperature, (c) Al–Cu–Fe–Cr coating D sprayed with the higher spraying temperature. i_1 denotes the icosahedral $Al_{80}Cr_{13.5}Fe_{6.5}$ phase, i_2 denotes the icosahedral $Al_{13}Cr_3Cu_4$ phase, θ stands for the tetragonal Al_2Cu phase and d stands for the decagonal phase in the Al–Cu–Fe–Cr system.

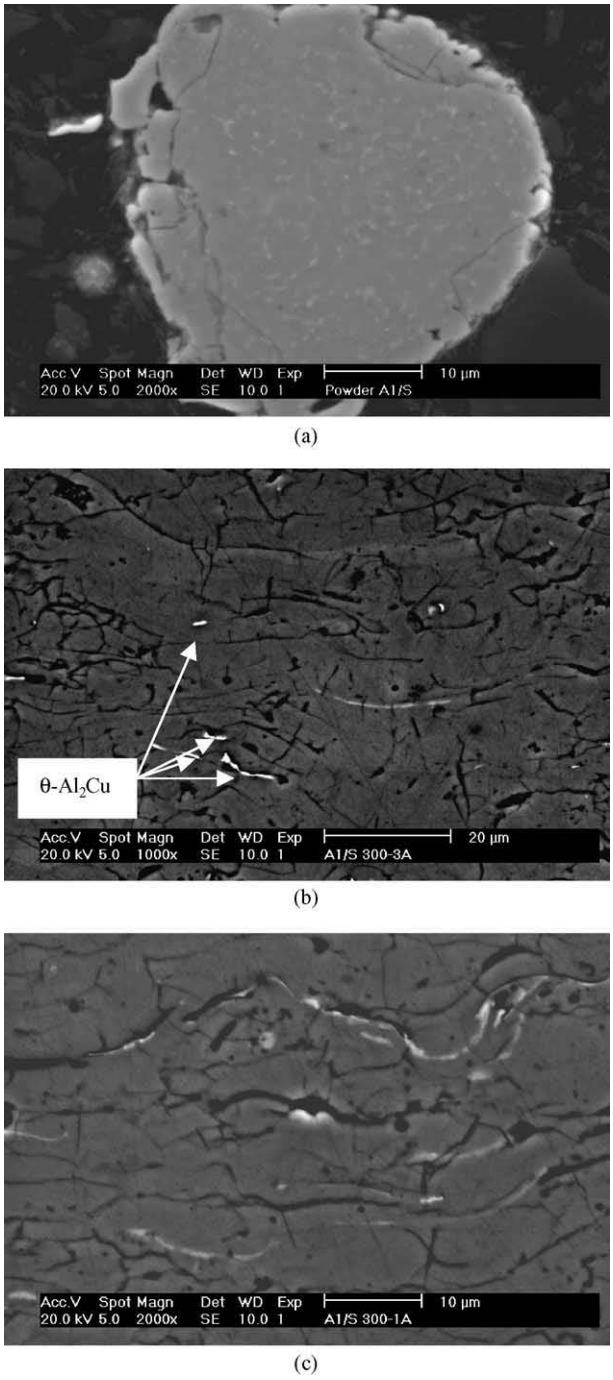

Fig. 5. SEM photographs showing the microstructural details of the Al–Cu–Fe–Cr feed powder and the HVOF sprayed coatings. (a) The morphology and microstructure of the Al–Cu–Fe–Cr feed powder F1. (b) The microstructure of the Al–Cu–Fe–Cr coating C deposited with the lower spraying temperature. (c) The microstructure of the Al–Cu–Fe–Cr coating D deposited with the higher spraying temperature.

The greater melting point of the Al–Cu–Fe–Cr feed power as compared to that of the Al–Cu–Fe feed powder was evidenced by differential thermal analysis (more detailed study of differential thermal analysis results is beyond the scope of the present study). It can, thus, be concluded that the Al–Cu–Fe–Cr powder particles were not melted completely during the spraying process. It is also worth noting that no oxidation was found to take place during the spraying process of the Al–Cu–Fe–Cr feed powder, independently of the spraying parameters. This contrasts sharply with the observations made for the Al–Cu–Fe coatings. Based on these results, it is suggested that the microstructure of the Al–Cu–Fe–Cr coatings is less sensitive to small changes in spraying temperature than the microstructure of the Al–Cu–Fe coatings.

ATEM studies were conducted for the Al–Cu–Fe–Cr feed powder and coatings C and D. However, due to the heavy charging of the feed powder under the electron beam, the microstructure of the feed powder could not be analysed with TEM. The coating particles were also charged in some degree, but the charging was not as intense as for the feed powder.

Fig. 6a shows the microstructure of the Al–Cu–Fe–Cr coating C viewed from the top of the coating. As can be noticed, the coating lamellas consisted of rather equiaxed grains of various sizes. This also applies to coating D. Both coating structures were found in ATEM examination to be composed of two different icosahedral phases (Fig. 6b and c). ATEM examination revealed the crushed coating particles to be mainly composed of either of these icosahedral phases. Both of them occurred seldom in the same particle. However, it is worth noting that no tetragonal θ-Al_2Cu phase could be encountered in either of the coating structures in ATEM studies.

The major phase in the coating C was detected to be the icosahedral phase i_1-$Al_{80}Cr_{13.5}Fe_{6.5}$ with the composition of 74.7 at.% Al, 10.1 at.% Cu, 7.4 at.% Fe and 7.8 at.% Cr. The electron diffraction pattern of this i_1-$Al_{80}Cr_{13.5}Fe_{6.5}$ phase from the fivefold axis is shown in Fig. 6b. The minor phase was the i_2-$Al_{13}Cr_3Cu_4$ phase, the composition of which was 66.5 at.% Al, 13.5 at.% Cu, 9.5 at.% Fe and 10.5 at.% Cr. The electron diffraction patterns of this i_2-$Al_{13}Cr_3Cu_4$ phase from five- and threefold axes are shown in Fig. 6c and d, respectively. In the coating D, in contrast, the icosahedral i_2-$Al_{13}Cr_3Cu_4$ phase was observed to be the major phase, with the composition of 60.5 at.% Al, 15.8 at.% Cu, 11.5 at.% Fe and 12.3 at.% Cr. The icosahedral i_1-$Al_{80}Cr_{13.5}Fe_{6.5}$ phase was the minor phase in the coating D. It exhibited a composition of 73.0 at.% Al, 10.5 at.% Cu, 7.9 at.% Fe and 8.5 at.% Cr.

4. Discussion

4.1. Microstructure of HVOF sprayed Al–Cu–Fe and Al–Cu–Fe–Cr coatings in the light of earlier coating studies

As compared to earlier studies on thermally sprayed Al–Cu–Fe coatings, deposited by plasma spraying, the phase structure of the studied HVOF sprayed Al–Cu–

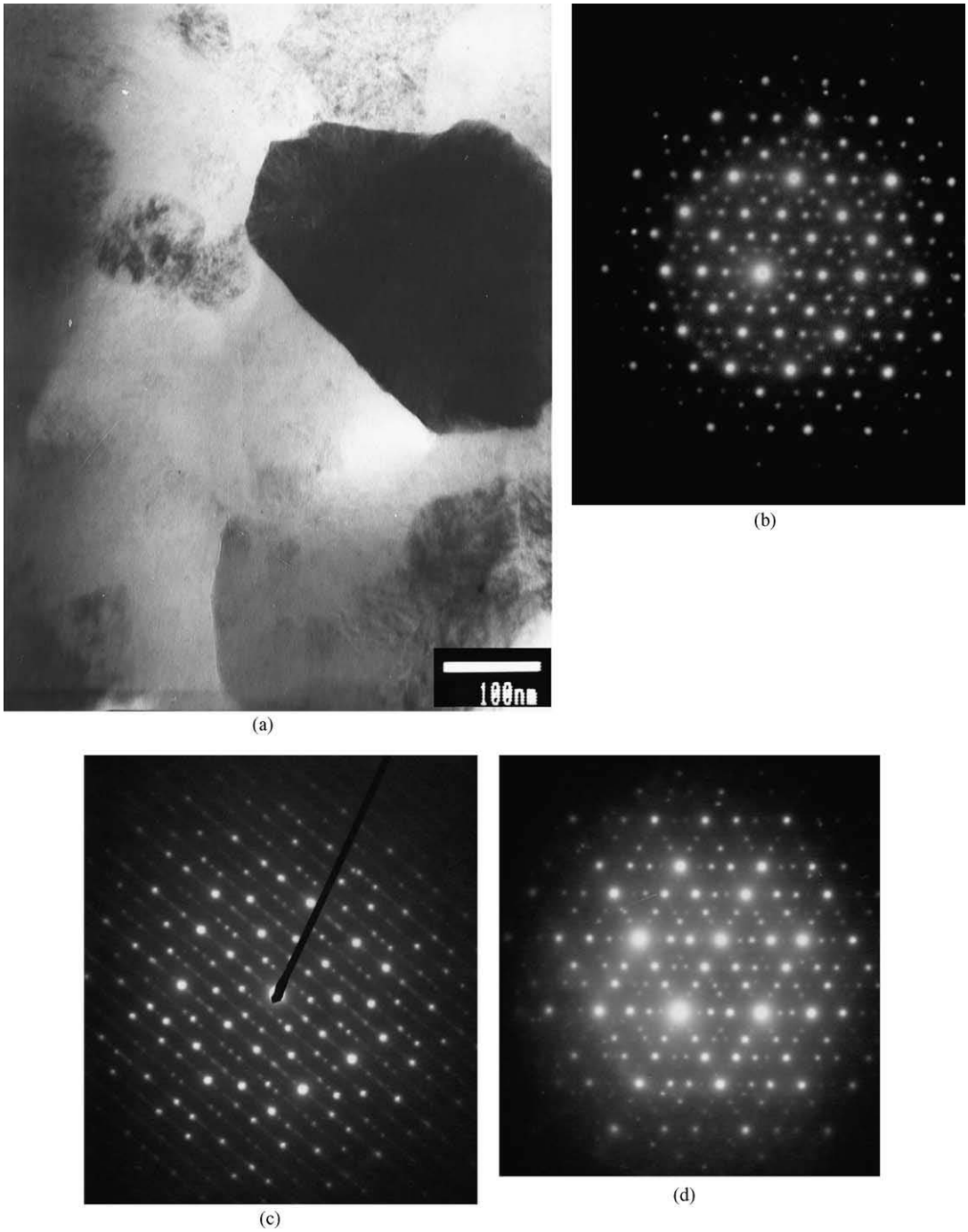

Fig. 6. Microstructure of the Al–Cu–Fe–Cr coating C sprayed with the lower spraying temperature. (a) TEM bright field image showing the coating structure from the top of the coating. Micrograph taken with the electron beam parallel to the fivefold axis of the dark grain. (b) Electron diffraction pattern of the major icosahedral i_1-$Al_{80}Cr_{13.5}Fe_{6.5}$ phase, taken along the fivefold axis. (c) Electron diffraction pattern of the minor icosahedral i_2-$Al_{13}Cr_3Cu_4$ phase, taken along the fivefold axis. (d) Electron diffraction pattern of the minor icosahedral i_2-$Al_{13}Cr_3Cu_4$ phase, taken along the threefold axis.

Fe coatings shows quite similar features. The HVOF sprayed coatings of the study are made up of the crystalline β-AlFe phase and the quasicrystalline i-$Al_{65}Cu_{20}Fe_{15}$ phase, which is in agreement with the earlier studies [8,17–19,23]. Only in one study [19], the formation of the λ-$Al_{13}Fe_4$ phase has been encountered in Al–Cu–Fe coatings in addition to the β-AlFe and i-$Al_{65}Cu_{20}Fe_{15}$ phases. Furthermore, oxygen has been detected both in the coatings of the present study and those reported in the earlier studies. Still, no pure aluminium oxide can be found in the HVOF sprayed Al–Cu–Fe coatings in this study or in the plasma-sprayed coatings of other studies. Oxygen is, therefore, incorporated in the coating structure rather as an oxidised form

of alloy present at lamella boundaries than a precipitated pure aluminium oxide phase [19].

Only Sordelet et al. [19] have earlier determined the composition of the phases present in thermally sprayed Al–Cu–Fe coatings. According to Sordelet et al., the average compositions of the neighbouring grains of the β-AlFe and i-$Al_{65}Cu_{20}Fe_{15}$ phases were 65.7 at.% Al, 21.9 at.% Cu and 12.5 at.% Fe and 73.9 at.% Al, 7.3 at.% Cu and 18.9 at.% Fe, respectively. The β-AlFe phase of the present study shows much higher amount of Cu as compared to the results of Sordelet et al. Similarly, the i-$Al_{65}Cu_{20}Fe_{15}$ phase of the coatings of this study is enriched in Cu as compared to that in the coatings of Sordelet et al. The composition of the feed powder is quite equal in our study and in the study of Sordelet et al., so it cannot be treated as a reason for the compositional difference of the coating phases. Besides, the Fe contents of the phases studied by us and by Sordelet et al. are of the same magnitude, suggesting that an excessive Al vaporisation cannot be a cause for the high Cu content of the coating phases of the present study. It is, however, important to keep in mind that the composition and volume ratio of coexisting phases as well as the spraying conditions all influence the composition of phases building the coating structure. As mentioned in the previous chapter, in the coatings of Sordelet et al., the λ-$Al_{13}Fe_4$ phase co-exists with the β-AlFe and i-$Al_{65}Cu_{20}Fe_{15}$ phases, while the coatings of the present study only contain the β-AlFe and i-$Al_{65}Cu_{20}Fe_{15}$ phases.

In addition to this compositional difference of the coating phases, the porosity level of the HVOF sprayed coatings of this study does not match with the earlier reported porosity levels in plasma- sprayed coatings. Based on the visual evaluation of the SEM photographs of the studied Al–Cu–Fe coatings, their porosity level is well below 10%. In plasma sprayed coatings, in contrast, porosities well above 10% are reported [17]. However, HVOF spraying generally introduces less porosity in coatings than plasma spraying, which is suggested to be the main reason for the difference in porosity level between the coatings of the study and those examined in earlier studies.

For the Al–Cu–Fe–Cr coatings of this study, the comparative data is mainly composed of earlier studies on the plasma-sprayed coatings [20,21] with one study concerning also HVOF sprayed coatings [24]. On one hand, according to Kong et al. [20], the as-sprayed coatings show a mixture of quasicrystalline and crystalline phases. Fleury et al. [24] have obtained similar results. They have specified these quasicrystalline phases to be icosahedrally and decagonally structured, while the crystalline phases refer to the quasicrystal approximant phases, the λ-$Al_{13}Fe_4$ phase and the β-AlFe phase. On the other hand, Dubois et al. [21] and Sordelet et al. [25] have shown that thermally sprayed Al–Cu–Fe–Cr coatings are only composed of quasicrystalline icosahedral and decagonal phases, with oxide particles present in the splat boundaries. This icosahedral phase is reported to be made up of 63.1 at.% Al, 24.6 at.% Cu, 11.6 at.% Fe and 0.7 at.% Cr. The composition of the icosahedral phase indicates it to be the one also occurring in the ternary Al-Cu-Fe system, i.e. the i-$Al_{65}Cu_{20}Fe_{15}$ phase. No exact composition of the quaternary decagonal phase, in contrast, is described [21]. The HVOF sprayed Al–Cu–Fe–Cr coatings of the present study, however, do not show the formation of any of the above-mentioned crystalline or quasicrystalline phases. In our study, the quasicrystalline i_1-$Al_{80}Cr_{13.5}Fe_{6.5}$ and i_2-$Al_{13}Cr_3Cu_4$ phases are encountered. The only crystalline phase found in our coatings is the θ-Al_2Cu phase. The marked differences between the icosahedral phases found in the coatings of this study and the earlier ones are suggested to be explained by the limited amount of data available for the Al–Cu–Fe–Cr quaternary system. The above-mentioned coating studies seem to comprise the majority of known literature on the Al–Cu–Fe–Cr quasicrystalline alloys. No proper phase diagrams, for example, exist for the system Al–Cu–Fe–Cr. Furthermore, the build-up of the decagonal phase is reported [21] to be heavily cooling-rate-dependent. The absence of this decagonal phase in our Al–Cu–Fe–Cr coatings is explained by a rather low cooling rate caused by the employment of low carbon steel substrates, the thermal conductivity of which is not sufficiently high (if compared for example to aluminium).

4.2. Influence of Cr alloying on the microstructure of HVOF sprayed Al–Cu–Fe coatings

Based on the Al–Cu–Fe phase diagram sketched by Faudot et al. [26], the feed powder of the observed composition of 56.3 at.% Al, 29.3 at.% Cu and 14.5 at.% Fe falls within the two-phase range of the β-AlFe and i-$Al_{65}Cu_{20}Fe_{15}$ phases, with somewhat equal phase amounts. The coexistence of these phases in the HVOF sprayed coatings of the study is, thus, in agreement with theory. Unfortunately, the corresponding information is not available for the Al–Cu–Fe–Cr system. It is, however, known that in Al–Cu–Fe–Cr alloys, quaternary icosahedral and decagonal phases as well as quaternary polymorphous quasicrystal approximants may exist. Also, a ternary icosahedral phase and many binary crystalline phases can be encountered in the Al–Cu–Fe–Cr system. Nevertheless, both reported icosahedral phases refer to the icosahedral phase existing also in the Al–Cu–Fe ternary system, the i-$Al_{65}Cu_{20}Fe_{15}$ phase, which may contain less than one percent Cr. In addition, the binary crystalline phases are the same as for the ternary Al–Cu–Fe system [21]. Our interest, therefore, lies mainly on the crystalline approximant structures of quasicrystals. The quasicrystal approximant phases in the Al–Cu–Fe–Cr alloys are determined to be

orthorhombically structured, with the alloying element concentrations varying from 5.0 at.% to 15.7 at.% Cu, from 10.0 at.% to 11.3 at.% Fe and from 7.1 at.% to 12.5 at.% Cr [21].

In this study, it is shown that the alloying of Al–Cu–Fe with Cr introduces two new ternary icosahedral phases, the i_1-$Al_{80}Cr_{13.5}Fe_{6.5}$ and i_2-$Al_{13}Cr_3Cu_4$ phases. In this study, the composition of the i_1-$Al_{80}Cr_{13.5}Fe_{6.5}$ phase is determined to be approximately 73.9 at.% Al, 10.3 at.% Cu, 7.7 at.% Fe and 8.2 at.% Cr. The composition of the i_2-$Al_{13}Cr_3Cu_4$ phase, in turn, is 63.5 at.% Al, 14.7 at.% Cu, 10.5 at.% Fe and 11.4 at.% Cr. These compositions are very close to those of the crystalline approximant phases reported by Dubois et al. [21]. Keeping in mind the fact that in the connection of the icosahedral i-$Al_{65}Cu_{20}Fe_{15}$ phase, the quasicrystal approximant phases form as a result of the annealing of a metastable quasicrystalline structure [27], it is suggested that there might be some structural relation between the new icosahedral phases identified in the HVOF sprayed coatings of the study and the approximant phases reported by Dubois et al. [21]. Nevertheless, it is sure that the addition of Cr to the Al–Cu–Fe alloy neither destabilises the icosahedral phase nor promotes the formation of the decagonal phase, as suggested by Dong and Dubois [28]. Instead, new icosahedral phases are introduced as a result of Cr addition to the Al–Cu–Fe alloy.

As for the structural characteristics of studied coatings, Cr addition to the Al–Cu–Fe alloy stabilises the quasicrystalline icosahedral phase yielding an almost completely quasicrystalline structure in the Al–Cu–Fe–Cr coatings, instead of a mostly crystalline structure of the Al–Cu–Fe coating. This stabilising influence of Cr alloying on the Al–Cu–Fe coating structure is also reflected in the negligible oxidation of the Al–Cu–Fe–Cr alloy during the spraying process as compared to the extensive oxidation of the Al–Cu–Fe alloy. Accordingly, the Al–Cu–Fe coatings contain oxide layers on the lamella boundaries. This build-up of an oxide layer on the splat boundaries has been shown to be typical for Al–Cu–Fe coatings [18,19], but also for Al–Cu–Fe–Cr [25] and for example for Al–Co–Fe–Cr [29] coatings as a result of a high-temperature spraying process. However, the oxidation of Al–Cu–Fe–Cr alloy during the coating process has been reported for coatings comprising of icosahedral and decagonal phases, the icosahedral one referring to the i-$Al_{65}Cu_{20}Fe_{15}$ phase existing in the ternary Al–Cu–Fe system, too. On the basis of the results obtained in this study, we suggest that the new icosahedral phases in the quaternary Al–Cu–Fe–Cr system, the i_1-$Al_{80}Cr_{13.5}Fe_{6.5}$ and i_2-$Al_{13}Cr_3Cu_4$ phases, are structurally more stable than the i-$Al_{65}Cu_{20}Fe_{15}$ phase and the quaternary decagonal phase existing in Al–Cu–Fe–Cr alloys. This structural stability introduces negligible oxidation during the HVOF spraying of the Al–Cu–Fe–Cr feed powder and the nearly oxide-free Al–Cu–Fe–Cr coating.

It is worth noting that as a result of spraying temperature change, no change in the influence of Cr alloying on the microstructure or phase selection of the Al–Cu–Fe coatings is introduced. The only notable difference brought about by the increased spraying temperature in the Al–Cu–Fe–Cr coatings is a minor shift in the volume ratio of the formed phases. In the Al–Cu–Fe–Cr coatings, the amount of the chromium-rich i_2-$Al_{13}Cr_3Cu_4$ phase somewhat increases as a result of higher spraying temperature, at the expense of the i_1-$Al_{80}Cr_{13.5}Fe_{6.5}$ phase and the remaining θ-Al_2Cu phase. No change in the oxidation behaviour can be observed in the Al–Cu–Fe–Cr coatings due to the raised spraying temperature. In the Al–Cu–Fe coatings, in turn, higher spraying temperature yields somewhat less quasicrystalline i-$Al_{65}Cu_{20}Fe_{15}$ phase as compared to the lower spraying temperature. The amount of the oxidised lamella boundaries simultaneously multiplies.

5. Conclusions

In this study, Al–Cu–Fe and Al–Cu–Fe–Cr thick coatings were deposited under different spraying conditions by a HVOF spraying technique to gain information on the influence of chromium alloying on the microstructure of HVOF sprayed quasicrystalline Al–Cu–Fe coatings in different spraying temperatures. The results obtained may be summarised as follows:

1. HVOF sprayed Al–Cu–Fe coatings are build up of lamellas of the crystalline β-AlFe phase. Individual particles of the quasicrystalline i-$Al_{65}Cu_{20}Fe_{15}$ phase exist between coating lamellas. Furthermore, the lamella boundaries are covered by an oxide layer. This oxide is not pure aluminium oxide but an oxidised form of either or both of the main phases. Due to the increased spraying temperature, the amount of the quasicrystalline phase is somewhat reduced and that of the oxide phase increased.
2. HVOF sprayed Al–Cu–Fe–Cr coatings are made up of the crystalline θ-Al_2Cu phase and two icosahedral phases, the i_1-$Al_{80}Cr_{13.5}Fe_{6.5}$ and i_2-$Al_{13}Cr_3Cu_4$ phases. As a result of the raised spraying temperature, the θ-Al_2Cu phase disappears, increasing the relative amount of the Cu-rich i_2-$Al_{13}Cr_3Cu_4$ phase. Coating lamellas are found to be composed of the icosahedral phases so that in one crushed coating particle, only either of these phases is detected. No oxide layer forms at the coating lamella surfaces.
3. HVOF spraying technique yields Al–Cu–Fe and Al–Cu–Fe–Cr coatings that are structurally

almost identical to those reported in literature, although they have been produced by plasma spraying. However, HVOF spraying introduces less porosity in coatings as plasma spraying. The porosity levels of the Al–Cu–Fe and Al–Cu–Fe–Cr coatings of the study were, thus, lower than those reported for plasma-sprayed coatings.

4. The present study provides new and complementary information on the phases occurring in a quaternary Al–Cu–Fe–Cr system. In addition to the icosahedral i-$Al_{65}Cu_{20}Fe_{15}$ phase, which also appears in the Al–Cu–Fe system, the icosahedral i_1-$Al_{80}Cr_{13.5}Fe_{6.5}$ and i_2-$Al_{13}Cr_3Cu_4$ phases exist in the Al–Cu–Fe–Cr alloys. The composition of the i_1-$Al_{80}Cr_{13.5}Fe_{6.5}$ phase is approximately 73.9 at.% Al, 10.3 at.% Cu, 7.7 at.% Fe and 8.2 at.% Cr, while that of the i_2-$Al_{13}Cr_3Cu_4$ phase is 63.5 at% Al, 14.7 at.% Cu, 10.5 at.% Fe and 11.4 at.% Cr. Earlier, the phases with these compositions are referred to be crystalline approximant phases of quasicrystals.
5. Cr addition to the Al–Cu–Fe coatings neither destabilises the icosahedral phase nor promotes the formation of the decagonal phase, as earlier suggested. Instead, new icosahedral phases are introduced as a result of the Cr addition to the Al–Cu–Fe alloy. It can, thus, be suggested that the icosahedral phase structure is stabilised by the Cr addition to the Al–Cu–Fe alloys.

Acknowledgements

E. H.-S. is deeply indebted to the Academy of Finland and Walter Ahlström Foundation for financing her research.

References

[1] Shechtman D, Blech I, Gratias D, Cahn JW. Phys Rev Lett 1984; 53:1951.
[2] Sordelet DJ, Dubois JM. Mater Res Soc Bull 1997;11:34.
[3] Wolf B, Bambauer KO, Paufler P. Mater Sci Engng 2001; A298:284.
[4] Jenks CJ, Thiel PA. Mater Res Soc Bull 1997;11:55.
[5] Dubois JM. Mater Sci Engng 2000;A294-296:4.
[6] Belin-Ferré E, Dubois JM, Fournée V, Brunet P, Sordelet DJ, Zhang LM. Mater Sci Engng 2000;A294-296:818.
[7] Brunet P, Zhang LM, Sordelet DJ, Besser M, Dubois JM. Mater Sci Engng 2000;A294-296:74.
[8] Sordelet DJ, Besser MF, Logsdon JL. Mater Sci Engng 1998; A255:54.
[9] Rapp Ö. Mater Sci Engng 2000;A294-296:458.
[10] Kimura K, Yamane H, Hashimoto T, Takeuchi S. Mater Sci Engng 1988;A99:435.
[11] Archambault P, Janot C. Mater Res Soc Bull 1997;11:48.
[12] Bilusic A, Pavuna D, Smontara A. Vacuum 2001;61:345.
[13] Bilusic A, Smontara A, Lasjaunias JC, Ivkov J, Calvayrac Y. Mater Sci and Engng 2000;A294-296:706.
[14] Eisenhammer T, Mahr A, Haugeneder A, Assmann W. Solar Energy Mater Solar Cells 1997;46:53.
[15] Kang SS, Dubois JM. Phil Mag 1992;A66:151.
[16] Urban K, Feuerbacher M, Wollgarten M. Mater Res Soc Bull 1997;11:65.
[17] Fleury E, Lee SM, Kim WT, Kim DH. J Non-Crystalline Solids 2000;278:194.
[18] Sordelet DJ, Besser MF, Anderson IE. J Thermal Spray Technol 1996;5:161.
[19] Sordelet DJ, Kramer MJ, Unal O. J Thermal Spray Technol 1995;4:235.
[20] Kong J, Zhou C, Gong S, Xu H. Surf Coatings Technol 2003; 165:281.
[21] Dubois JM, Proner A, Bucaille B, Cathonnet Ph, Dong C, Richard V, et al. Annales de Chimie-Sciences des Materiaux France 1994;19:3.
[22] Pawlowski L. The science and engineering of thermal spray coatings. Chichester, UK: John Wiley & Sons; 1995.
[23] De Palo S, Usmani S, Sampath S, Sordelet DJ, Besser M. Thermal spray. A united forum for scientific and technological advances. Ohio, USA: ASM; 1997 p. 135.
[24] Fleury E, Kim YC, Kim JS, Kim DH, Kim WT, Ahn HS, et al. J Alloys Compounds 2002;342:321.
[25] Sordelet DJ, Widener SD, Tang Y, Besser MF. Mater Sci Engng 2000;A294-296:834.
[26] Faudot F, Quivy A, Calvayrac Y, Gratias D, Harmelin M. Mater Sci Engng 1991;A133:383.
[27] Edagawa K, Waseda A, Kimura K, Ino H. Mater Sci Engng 1991;A134:939.
[28] Dong C, Dubois JM. J Mater Sci 1991;26:1647.
[29] Huttunen-Saarivirta E, Turunen E, Kallio M. J Alloys Compounds 2003;254:269.